JMEPEG (2024) 33:7253–7264
https://doi.org/10.1007/s11665-023-08445-9

©ASM International
1059-9495/$19.00

ORIGINAL RESEARCH ARTICLE

Characteristic of CuMn Alloy Films Prepared Using Electrochemical Deposition

Wen-Hsi Lee, Narendra Gharini Puteri, and C.R. Kuo

Submitted: 27 March 2023 / Revised: 2 June 2023 / Accepted: 11 June 2023 / Published online: 7 August 2023

Copper-manganese (Cu-Mn) alloys are usually used in resistance materials with a low resistance and low temperature coefficient of resistance (TCR). In the study, two kinds of electrochemical deposition methods were used to prepare a Cu-Mn structure. Firstly, high conductivity Cu film with preferred (111) orientation was prepared based on the Al thick film as the sacrificial layer by screen printing on the Al_2O_3 substrate, and then transformed the Al thick film into the Cu thick film by the galvanic displacement reaction at 80 °C for 75 min. Secondly, the electroplating method was used to deposit Mn on the as-replaced Cu film. it could be seen that a high quality and desired Cu-Mn 9:1 ratio could be obtained by depositing at 1.6 V for 10 min in $MnCl_2$ electrolyte with $(NH_4)_2SO_4$. Sequentially, annealing under normal pressure in reducing the atmosphere was done to make the Cu and Mn interdiffusion into the alloy phase. Both x-ray photoelectron spectroscopy and Raman confirmed that annealing at 900 °C in a nitrogen-hydrogen (95/5) atmosphere could extremely reduce the possibility of manganese oxidation and showed promising electrical properties including of the low temperature coefficient of resistance (TCR = 150 ppm) with resistivity of 1000 $\mu\Omega$-cm, which are comparable to that of CuMn deposited by sputtering in vacuum.

Keywords annealing, CuMn alloy, electrochemical deposition, resistance of thick film

1. Introduction

Although pure copper has ultra low resistivity, its temperature coefficient of resistance (TCR) is relatively high and against the application of resistors. To solve this issue, the alloy material receives much attention as it has the advantages of high thermal stability and mechanical properties. Copper-manganese alloy is one of the most potential alloy materials and it has been widely used in the modern industry. It has a low TCR, outstanding long-term stability and good weldability characteristics, which makes the alloy superior to precision surveying instruments (Ref 1, 2).

Even though the Cu-Mn alloy is a high potential material, its process restricts the development and application, since Mn has a high affinity for oxygen, so Mn is easily oxidized during thermal treatment. Among various physical synthesis methods for Cu-Mn thick films, sputtering has been widely used to prepare conductive films with controllable physical properties and high qualities (Ref 3-5). A co-sputtering method technique allows for a desired film thickness to be applied simply by controlling the process duration, and crystalline film alloy with controllable microstructures can be acquired through in situ crystal growth at different growing temperatures (Ref 6). However, compared to other chemical processes, its cost and multi-steps induce a low profit, which causes a bottleneck in the industry. In other words, the chemical process is a high-potential method for the CuMn alloy. There are varieties of methods for manufacturing CuMn alloy films including sputtering (Ref 7), sol–gel (Ref 8,), and electrodeposition (Ref 9). Among these processes, the alloy electrochemical deposition technique is widely used for the protection that requires special chemical, physical, and mechanical features due to its considerable characteristics of simplicity and lower cost in comparison to other methods. In the electrochemical plating process, there are several parameters deciding the properties of electroplated films such as current density, pH, deposition potentials, electrolyte concentration, electroplating time, and additives (Ref 10).

Aluminum thick film is one of the most promising materials for a CuMn alloy. First, Al electrode with pattern is formed by screen printing. And then, since the chemical potential of Al^{3+}/Al is − 1.66 V versus SHE, the Al electrode is prospective to be a sacrificial layer for some metals with high reduction potential such as Pd, Pt, Ag, Cu and Ni. On the other hand, the porous characterization of thick aluminum films allows total replacement (Ref 11). The conventional displacement method could only deposit a limited metal layer on the substrate due to the impact surface. The reaction will stop if it is covered with the deposited metal. The modified replacement is defined as being that the substrate based on the porous aluminum paste could penetrate the substrate and replace the material from bottom to top. Previous research has developed the copper and copper-nickel thick alloy film through the modified replacement method and many potential applications in electronic packages, passive components, or multilayer ceramic capacitors, etc. (Ref 12, 13). In this work, a CuMn alloy resistor can be realized through Al coating by screen printing and replaced with Cu by displacement chemical reaction. Sequentially, Mn is deposited

Wen-Hsi Lee, Narendra Gharini Puteri, and **C.R. Kuo**, Department of Electrical Engineering, National Cheng Kung University, Tainan, Taiwan, ROC. Contact e-mail: leewen@mail.ncku.edu.tw.

on Cu film by electroplating and then the CuMn alloy is formed by annealing process.

2. Experiments

2.1 Sample Preparation

Figure 1 shows a flow chart of the experiments. At first, the Al thick film was printed on the Al_2O_3 substrate by the Al paste which is made of 10 μm Al micro-particles, binder, and other additives. After printing, the Al film was fired at 750 °C in air to form a homogenous and flat structure. Next, the replacement of Cu film was conducted at 80 °C for 15, 30, 45, 60 and 75 min. The electrolyte consisted of 10 g $CuSO_4$ and tiny Polyvinylpyrrolidone (PVP), Ethylenediaminetetraacetic acid (EDTA) and bis(sodium-sulfopropyl) disulfide (SPS) in 50 ml DI water.

The following Mn-electroplating process would be based on the sample of Cu replacement for 60 min. It is well-known that a proper electroplating potential could prevent polarization during the process. Therefore, the plating potentials were applied from 1.5 to 1.8 V to find the optimization potential for the Cu replacement film. To provide the optimization of the Mn-based electrolyte, its electrochemical behavior must be realized to control some key process parameters, like the solution composition, electroplating potential, and pH value (Ref 14). It has been known that the ions of manganese could be only stably kept when the pH is below 7. Nevertheless, its electroplating efficiency would be affected with a slight change of pH value due to its high sensitivity. Therefore, a detailed investigation of the pH influence should be undertaken. Also, the coating rate would be confirmed by the Mn films deposited for 10 and 15 min. After that, the as-synthesized Cu-Mn structure was subsequently annealed in a 3N N_2 and another hydrogen-contained N_2 atmosphere for 1 hour at the temperatures of 400-900 °C to induce a solid-state reaction between the Cu and Mn.

2.2 Characterization

In this work, the scanning electron microscopy and Energy-dispersive x-ray spectroscopy (SEM EDS; temic) was used to observe the surface morphology of samples. The x-ray diffraction experiments (XRD; Philips PW1710 Cu Kα radiation) with range 20-80° was used to confirm the composition of the film. The Raman spectroscopy (Bruker Senterra Dispersive Raman) was performed at room temperature with range 200-900 cm^{-1} to confirm the intermolecular bond of the film with different gas for sintering. The x-ray photoelectron spectroscopy (XPS; Perkin Elmer Model 5500) was performed to investigate the chemical binding states of the constituent elements of the Cu-based alloy film. The electrochemical analysis was obtained by using linear swept voltammetry and cyclic voltammetry with sweep window − 1.8 to − 0.9 V. The sheet resistance *Rs* of each samples were measured by digital multimeter. The resistivity was calculated by using the four-point probe method. For calculating the TCR of the samples, each samples had to be soaked at the set tempearture for 5 minutes before measuring the resistance. After the value of the resistance at the designated temperature collected, the TCR can be calculated by the equation below where the resistance of R25 is 25 °C and the resistance of R125 is 125 °C:

$$\mathrm{TCR} = (R125 - R25)/(R25 \times 100) \qquad \text{(Eq 1)}$$

3. Results and Discussion

3.1 Preparation of Cu Layer by Galvanic Displacement with Al Thick Film

To confirm the time evolution of the Cu replacement from Al film, the surface morphology of the films with different replacement times is depicted in Fig. 2(a) to (d). Figure 2(a) demonstrates the original Al thick film without any treatment and some Al particles are stacked closely. After galvanic

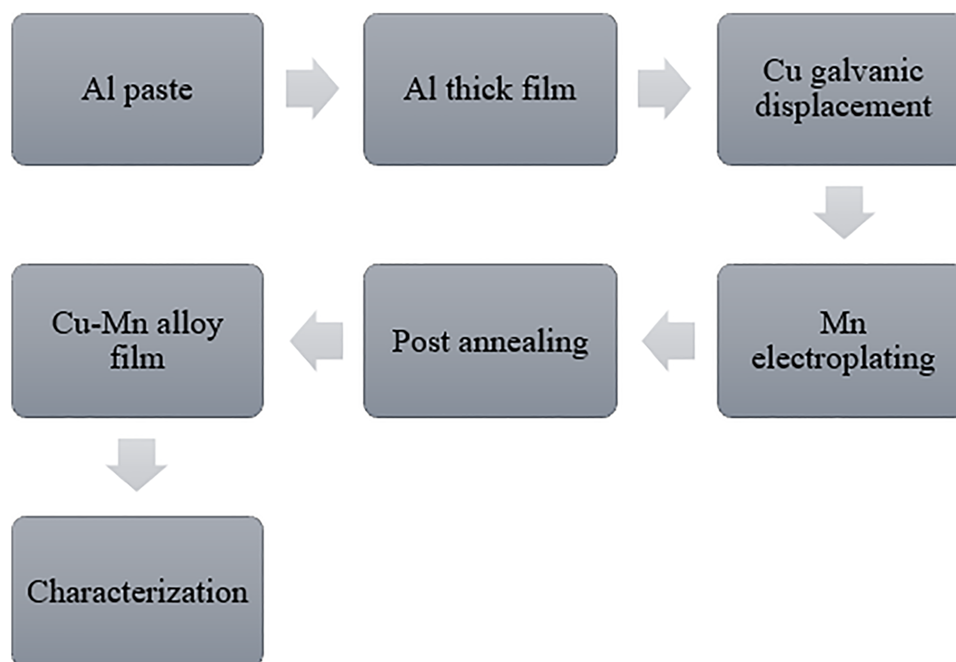

Fig. 1 Flow chart of experiments

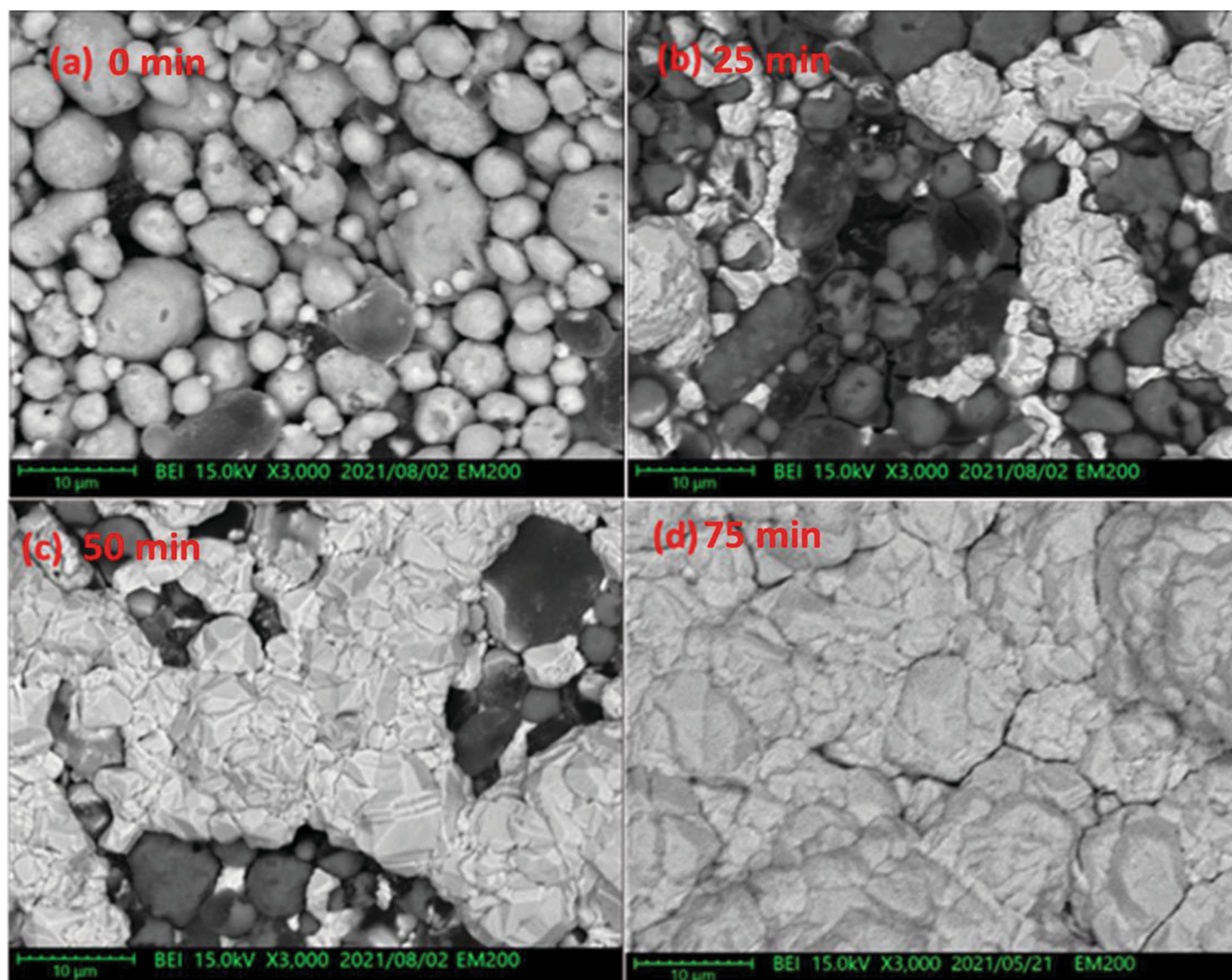

Fig. 2 (a), (b), (c) and (d) The top view of the Al thick film before and after the Cu galvanic displacement reaction for 25, 50 and 75 min, respectively

displacement for 25 min at 80 °C, some small Cu grains appeared at the top of the film and the original Al particles became uneven, implying that galvanic displacement has happened. As the galvanic displacement time increased, the surface of Al thick film was gradually covered with a Cu layer.

When the galvanic displacement reached 75 min, the feature of the Al particles had totally vanished.

This illustrated that the samples could reach the total-replacement in the 75 min process time.

The crystallographic structures of the Cu films with different galvanic displacement times were identified by XRD. The Bragg reflection as shown in Fig. 3 demonstrates that the Al thick film consists of the cubic Al (JCPDS No. 004-0787) and γ-Al_2O_3 of the hexagonal structure (JCPDS No. 046-1212) without an obvious orientation, implying that the thick film was crystallized under a relatively thermodynamic equilibrium. The spectra at 43.3°, 50.4° and 74.2° are ascribed to (111), (200) and (220) crystallographic planes of cubic Cu (JCPDS No. 004-0836), respectively. Well-crystallized Cu thick films were successfully formed via galvanic displacement based on the Al thick films and exhibited preferred (111) orientation with a high density and low resistance. This shows that the XRD patterns of the Cu film replaced from 25 to75 min, and that the intensity of the Cu peaks increased gradually as the galvanic displacement time increased (Ref 15), reflecting to that the proportion of Al replaced with Cu increased with increasing time.

3.2 Preparation of Mn Layer on Cu Layer by Electroplating

3.2.1 Effect of pH and Various Additives. The linear sweep voltammetry (LSV) scanning results of the Mn-based solution at different pH environments is depicted in Fig. 4. It can be seen that the open circuit potential (OCP) is − 0.821 V when the pH value of the solution is 2.4. Altough, as the pH value increased, the OCP became more negative. The pH limitation of our condition is at 6.7 and its OCP is − 0.834 V. With a more negative potential, the distance between the OCP and theoretical reduction potential decreased, and the current efficiency is enhanced during the electroplating.

Figure 5(a) exhibits the CV scans with various amounts of $(NH_4)_2SO_4$ from − 1.8 to − 0.9 V. A peak at − 1.01 V is shown in the positive scan, is attributed to the Mn oxidation. However, in the negative scan, there are no peaks observed and only a violent drop appeared over − 1.5 V. This drop is implying that an electroplating reaction was happening in that potential range. According to previous research (Ref 16), the reduction peak of manganese is at − 1.63 V and it is

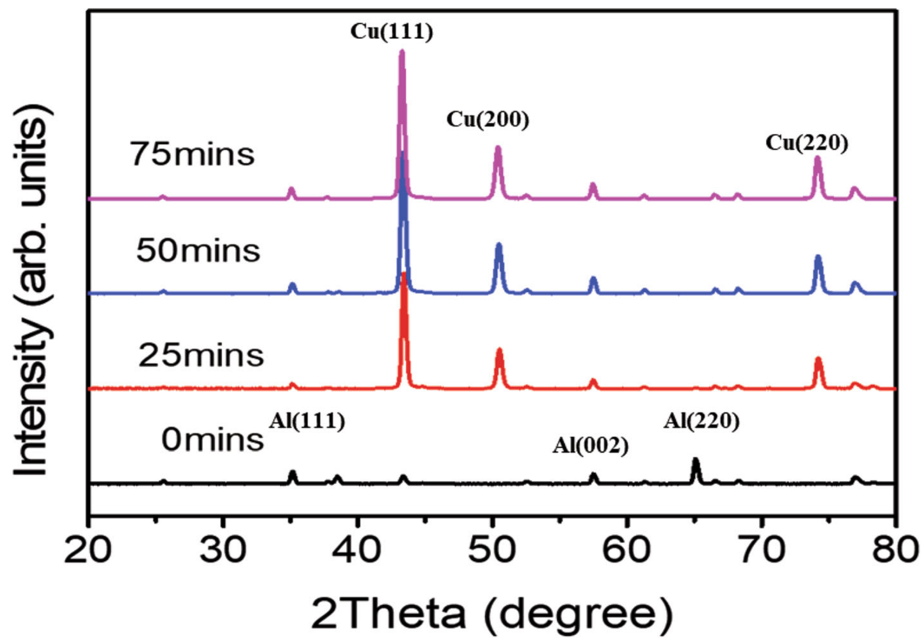

Fig. 3 XRD analysis on the Al thick film before and after the Cu galvanic displacement reaction for 25, 50 and 75 min, respectively

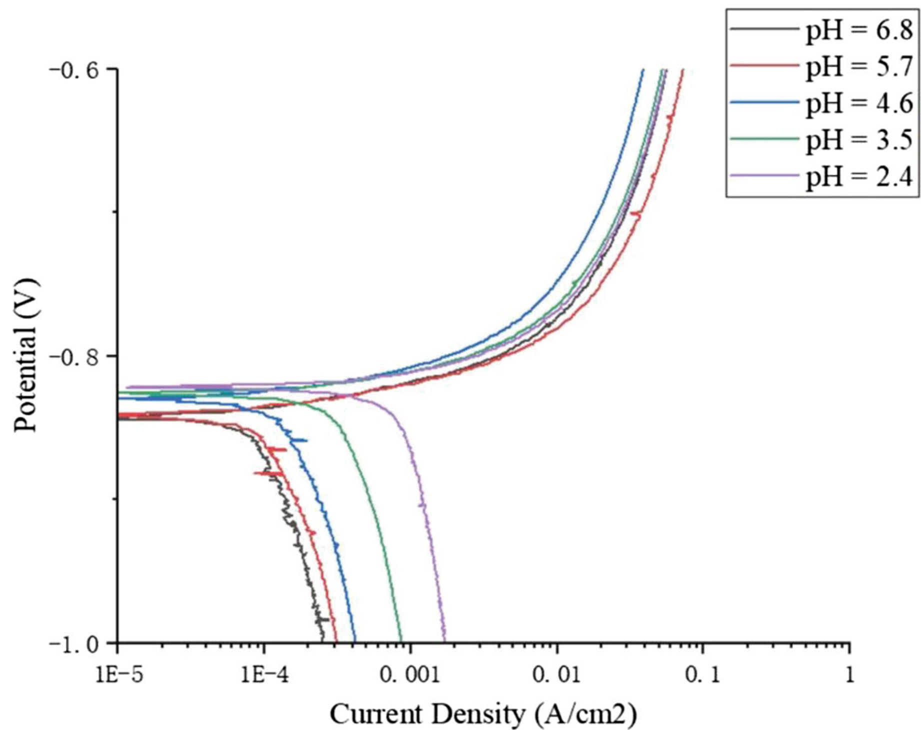

Fig. 4 Linear sweep voltammetry scans of the film in the Mn-based solution with different pH environments

overlapping with the electroplating curve. Hence, the redox reaction can be determined by the oxidation peak. As the concentration of $(NH_4)_2SO_4$ increased, the position shifted to a higher voltage and the intensity became weaker (Ref 10). It was shown that the coated Mn is more difficult to oxidize in a solution that includes $(NH_4)_2SO_4$. However, the efficiency of the electroplating should consider not only the stability but also the nucleation rate. With the various concentrations of $(NH_4)_2SO_4$, the 7 g/L $(NH_4)_2SO_4$ in the solution could provide better stability and electroplating efficiency. The additives used were Ethylene thiourea (ETU), Dimethyloldimethyl hydantoin (DMDMH) and a commercial mixed additive (K-additives) as shown in Fig. 5(b), (c) and (d), which applied copper electroplating and replacement. As seen on the figures, there are no huge impact to the result (Ref 17).

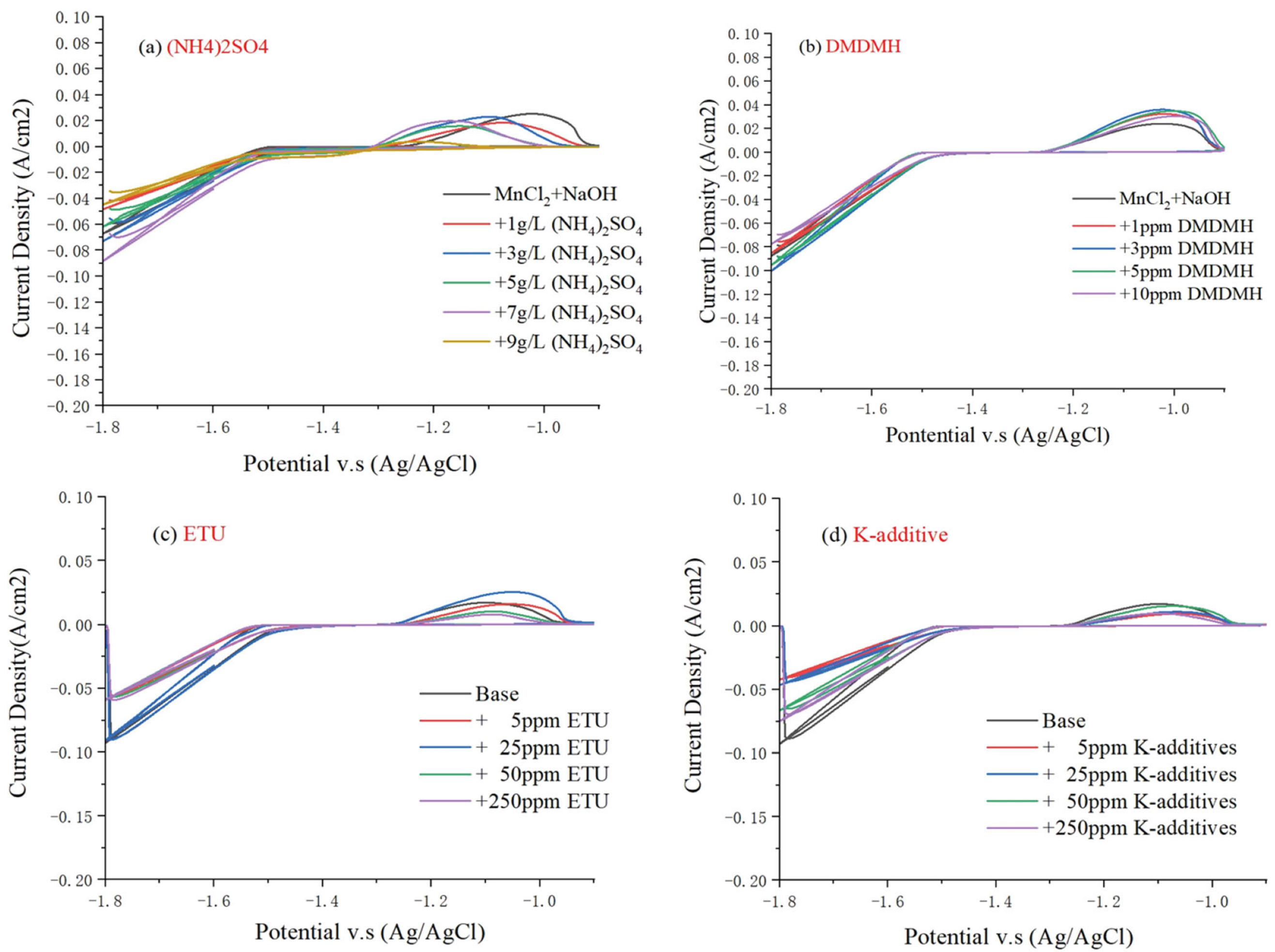

Fig. 5 (a), (b), (c) and (d) cyclic voltammetry scans of the film in the Mn-based solution with various $(NH_4)_2SO_4$ co, DMDMH. ETU and K-additive concentrations

3.2.2 Effect of the Electroplating Potential. The Mn layer coated on a Cu film under 1.5, 1.6, 1.7 and 1.8 V in 10 minutes were confirmed by SEM as shown in Fig. 6(a), (b), (c) and (d). Figure 6(a) shows the SEM micrographs of the deposition under 1.5 V and some islands with a rough surface were observed on the substrate. This could be attributed to the deposition of the impurities because it was destroyed under higher electroplating potential (Ref 18). When the potential increased to 1.6 V, the new deposition in Fig. 6(b) became uniform and the grains were visible with an average diameter of 1 μm. Corresponding to the elemental analysis, the coating should be the manganese and the tiny impurities that were absorbed on the surface or mixed between the grains. Further increasing the potential to 1.7 and 1.8 V seems to have no significant influence that shown in Fig. 6(c) and (d). From this experiment demonstrated that the potential of 1.6 V is enough for the deposition of the Mn film. Hence, the following experiment would apply this potential for the electroplating of the Mn layer.

3.2.3 Effect of the Electroplating Time. The Mn film coated on the replaced-Cu film was deposited at 1.6 V for 10 and 15 min and is shown in Fig. 7(a) and (b) respectively. When the deposition time is 10 min, the thickness of the Mn layer is reached up to 4 μm. Moreover, it was notable that an explosive growth of the thickness could be observed in the electroplating time 15 min in Fig. 7(b) with average thickness is 30 μm. The difference of the deposition rate is attributed to the nucleation mechanism during the electroplating reaction. At first, the Mn nucleation happened on the surface of the replaced-Cu film, so the reaction was relatively slow because of the heterogeneous nucleation. After awhile, the surface was covered with some Mn grains and the growth mechanism transferred to the second stage. The deposition prefers to occur around the as-formed Mn grains, which could be attributed to the homogeneous nucleation (Ref 19). Under this nucleation mechanism, the reaction rate would become higher due to lower activation energy. In other words, the deposition rate is higher with a seed layer. From the as-known condition, the Mn electroplating for 10 min is promising to form an alloy with a Cu-Mn 9:1 ratio, so the following annealing experiments are based on this condition.

3.2.4 Formation of CuMn Alloy Films by Annealing. After the annealing treatment to induce the solid state reaction between the replaced Cu and electroplating Mn, the XRD analysis was applied to determine the material structure. Figure 8(a) to (d) shows the XRD patterns of the CuMn films annealed at 450-900 °C in the N_2 atmosphere. Figure 8(a) indicates that the pattern of CuMn film is like the one of the

Fig. 6 (a), (b), (c) and (d)The top view of the electroplated Mn film on the replaced- Cu film under 1.5, 1.6, 1.7 and 1.8 V

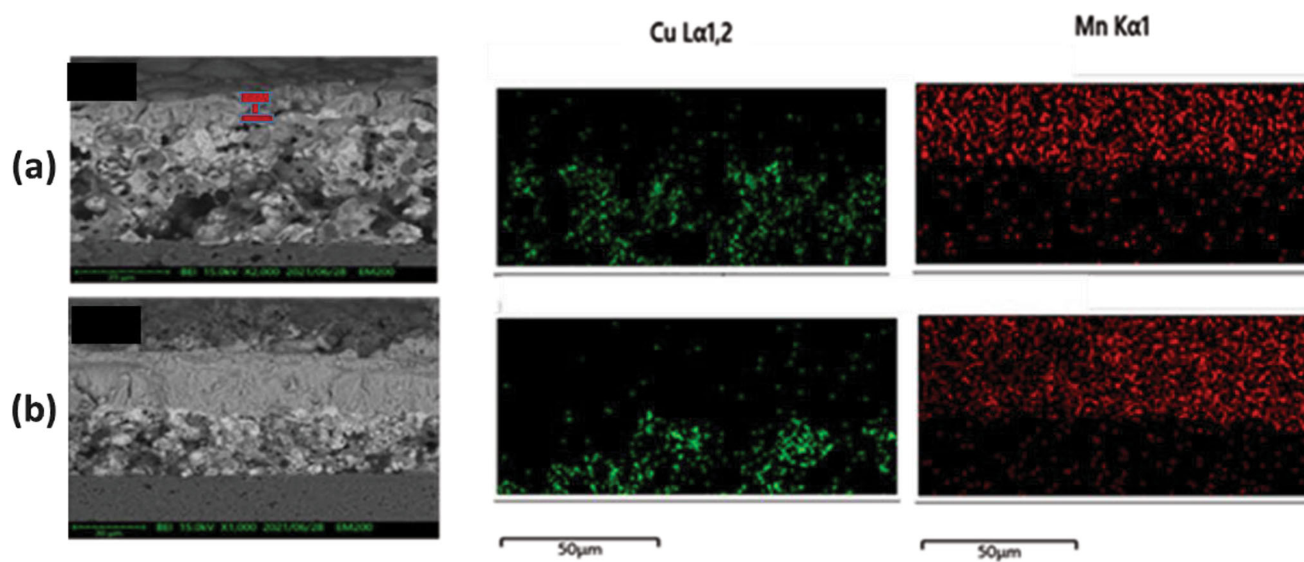

Fig. 7 (a) and (b). The co-section and element mapping of the electroplated Mn film on the replaced-Cu film under the 1.6 V for 10 min and 15 min

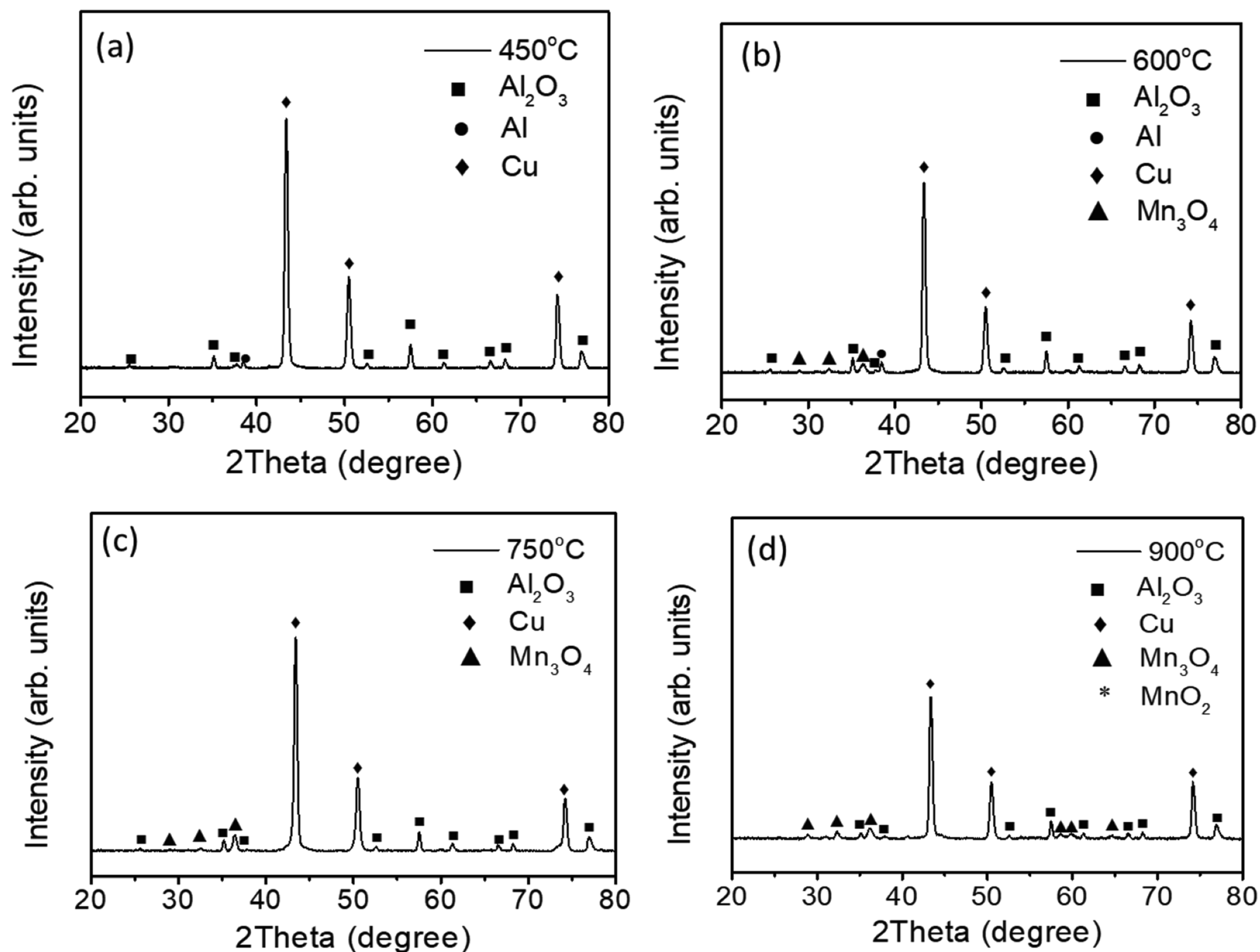

Fig. 8 (a), (b), (c) and (d) XRD pattern of CuMn films after annealing at different temperatures in N_2

unannealed sample. There are no new diffraction peaks in the diffraction pattern, illustrating that the driving force of the heat is still not enough for the oxidation or the other solid-state reaction. It has been reported that no peaks belong to the CuMn phase. However, since manganese is apt to oxidize even if the environment only contains a tiny amount of oxygen (Ref 20), the appearance of the Mn-based oxides could be regarded as the Mn element has been separated from the CuMn alloy film and precipitated onto the surface.

The XRD pattern of the CuMn alloy film annealed at 600 °C in an N_2 atmosphere in Fig. 8(b) illustrates the original peaks attributed to the Cu film decreased slightly and several new diffraction peaks emerged at approximately 29.0°, 32.4° and 36.4° which could be assigned to (112), (103) and (200) planes of the tetragonal Mn_3O_4 structure (JCPDS No. 024-0734), respectively. The existence of Mn_3O_4 demonstrates that the CuMn film would start deteriorating in the N_2 environment if the annealing temperature was higher than 600 °C. Figure 8(c) shows the XRD pattern of the CuMn alloy film annealed at 750 °C. It seems that the Cu and Mn element didn't develop a further reaction because no new peak appears in the diffraction pattern. The vanishment of the Al peaks is attributed to the annealing temperature having been higher than the melting point of Al. It causes the residual Al particles to melt in the annealing process and re-oxidize in the cooling process. Similarly, when the residual Al prefers to form oxides, it is very difficult to diffuse into the Cu crystal and act as substitute atoms for the Al atoms. Therefore, the oxidation of the Al would not affect the formation of the CuMn alloy. Next, when the annealing temperature increases to 900 °C, there is one new diffraction peak at 40.9° as shown in Fig. 8(d) which could be assigned to the (200) plane of the tetragonal MnO_2 structure (JCPDS no. 004-0591). The XRD results indicate that CuMn alloy cannot be formed by annealing in N_2 atmosphere at high temperature due to the fact of Mn oxidation or the annealing temperature is not high enough for the interdiffusion (Ref 21).

To confirm the feasibility of a hydrogen-containing annealing atmosphere, Raman spectroscopy was used to analyze the vibrational properties related to the grain boundary phase of CuMn alloy films without and with an annealing process in N_2 or N_2-H_2 as shown in Fig. 9. There are no peaks seen in the CuMn alloy film without annealing graph, which illustrated that the as-deposited films didn't present metal-oxygen bonds. It is noted that the as-prepared CuMn films could be maintained in a metallic state in an air environment. After annealing in N_2, the Raman spectrum of the films engendered three main peaks at about 316, 371 and 655 cm^{-1}, which are in good agreement with the literature data for Hausmannite Mn_3O_4 (Ref 22). The strongest peak at around 655 cm^{-1} in the Raman spectra of the annealed samples is the characteristic of all spinel structures

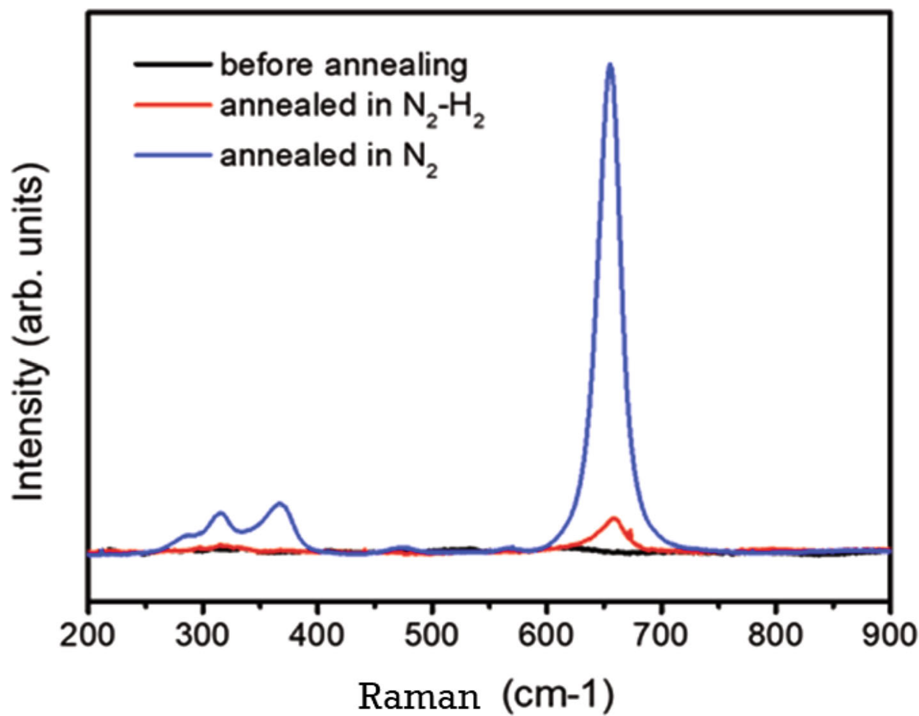

Fig. 9 Raman shift of the CuMn alloy films before and after annealing in N_2 and N_2-H_2

(Ref 23). This peak originated from a symmetrical stretching mode of the MnO_6 vibrational unit. However, the oxidation formation causes the precipitation of Mn from Cu, which leads to the separation between Cu and Mn. Raman spectra of the CuMn annealed in N_2-H_2. The peak belonged to the Mn-O bond at a 655 cm^{-1} decrease and even the peaks at 316 and 371 cm^{-1} almost vanished. It shows that the hydrogen-containing atmosphere could effectively reduce the oxidation for the Mn element during the annealing process. This result is consistent with the XRD analysis above.

XPS was used to study the element bonding state of CuMn composite film with and without H_2 during thermal annealing at 900 °C in N_2. The XPS survey spectrum in Fig. 10(a) shows the peaks of Cu, Mn, and O elements without impurity peaks. The narrow spectra of Cu 2*p* and Mn 2*p* of the CuMn composite film are shown in Fig. 10(a). The Cu 2*p* spectrum of the original Cu-Mn thin film in Fig. 5(b) consists of two spin-orbit doublets, which corresponds to the different valence states of copper (Ref 24). The larger doublets at 952.3 and 932.4 eV are attributed to Cu $2p^{1/2}$ and Cu $2p^{3/2}$ of Cu0, respectively, and the smaller doublets are assigned to Cu^+ . The asymmetric Mn 3*p* spectrum of the Cu-Mn composite film is shown in Fig. 10(a). The spectrum is deconvoluted into two sub-peaks at approximately 49.1 and 50.1 eV, which correspond to the trivalent and tetravalent states of manganese in the film matching, respectively. In contrast, in Fig. 10(a), the investigated spectra of Cu-Mn thin films containing H_2 during thermal annealing in N_2 at 900 °C show similar spectral characteristics to those shown in Fig. 10(b), indicating that in the post-annealing process no other pollution occurred. Figure 10(b) shows the Cu 2*p* spectrum of the film annealed in a hydrogen-containing atmosphere. Even if annealed in a reducing atmosphere, a monovalent Cu component will still appear on the surface of the alloy film under such annealing conditions. In contrast, the Cu 2*p* spectrum with deconvolution peaks in Fig. 10(b) show that the CuMn alloy film subjected to thermal annealing in N_2-H_2 shows that the area ratio of the Cu^+ spin-orbit doublet becomes smaller, which is due to the prevention of oxide being formed during the post-annealing process. The Mn 3*p* spectrum of the corresponding sample is shown in Fig. 10(b), which is used to explain the Cu 2*p* XPS results. The peak attributable to Mn 3*p* indicates a red shift during the hydrogen-containing annealing process, indicating the presence of metallic Mn in the CuMn film. The Mn 3*p* spectrum of the alloy film annealed in N_2-H_2 shows that compared with the trivalent and tetravalent states of manganese, the intensity of the metallic manganese sub-peaks is significantly increased, which is related to the trivalent and tetravalent states of manganese. The intensity of the sub-peak is relatively reduced from CuMn film annealed in N_2. The valence of manganese atoms is closely related to the morphology of the film. A similar phenomenon in which a CuMn alloy deteriorates during annealing has been proposed in previous work (Ref 25). According to Iijima et al. even 1 ppm of residual oxygen during the annealing process can oxidize Mn to MnOx (Ref 26). This phenomenon is very consistent with our findings. Although our annealing is carried out in a N_2 environment, the oxidation of Mn is still possible. The XPS results here show that the N_2-H_2 annealing atmosphere used for the CuMn alloy film allows more phase changes during the annealing process; manganese is still in a metal-bonded state and has not been reduced to a metal-bonded form.

Figure 11(a), (b) and (c) show microstructure and element mapping of CuMn film before and after annealing at 900 °C for 1 h in N_2.and in N_2-H_2.The results revealed that the grains on the surface were grown after annealing at 900 °C for 1 h in N_2.and in N_2-H_2. The films annealed in N_2 performed two forms of particles: one is larger and smooth and the other is smaller and covered with cracks, assigned to Cu and MnO_2 regions. Instead of separation, the films annealed in N_2-H_2

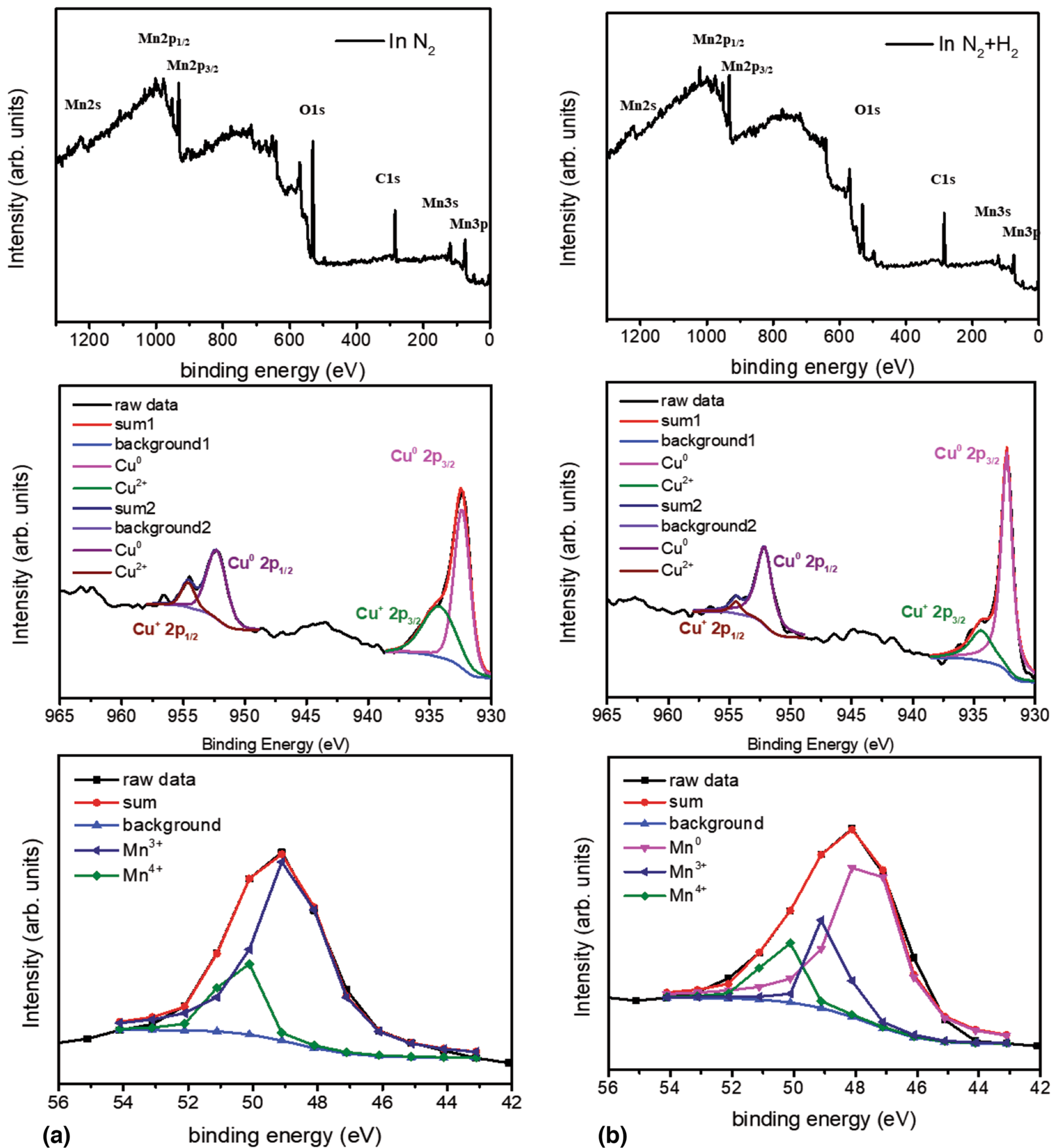

Fig. 10 (a) and (b) The survey scan spectra, the Cu 2*p* narrow scan spectra and the Mn 3*p* narrow scan spectra of the CuMn film annealed at 900 °C for 1 hr in N_2 and N_2+H_2

demonstrated an even and homogeneous surface, implying a good phase transformation of the CuMn alloy film through the Cu-Mn interdiffusion (Ref 27). Figure 11(b) shows the cross-section of Cu-Mn films after annealing at 900 °C in N_2 for 30 min, where no Mn atom diffusion is observed. On the other hand, Fig. 11(c) shows the cross-section of Cu-Mn films after annealing at 900 °C in N_2-H_2 for 30 min, where the Mn atoms continually diffuse into the interface and the grains of Cu also grow up at the same time. From the SEM analysis, we could observe that the CuMn films annealed with and without hydrogen in nitrogen performed different morphologies It seems that the oxidation of Mn plays an important role to determine the morphologies during thermal process.

There is a self-forming layer at the interface, and there are swellings in several places in these layers since the Mn atoms diffuse along the grain boundary (Ref 19, 28), and some of the atoms are trapped on the bottom of these paths. The chemical

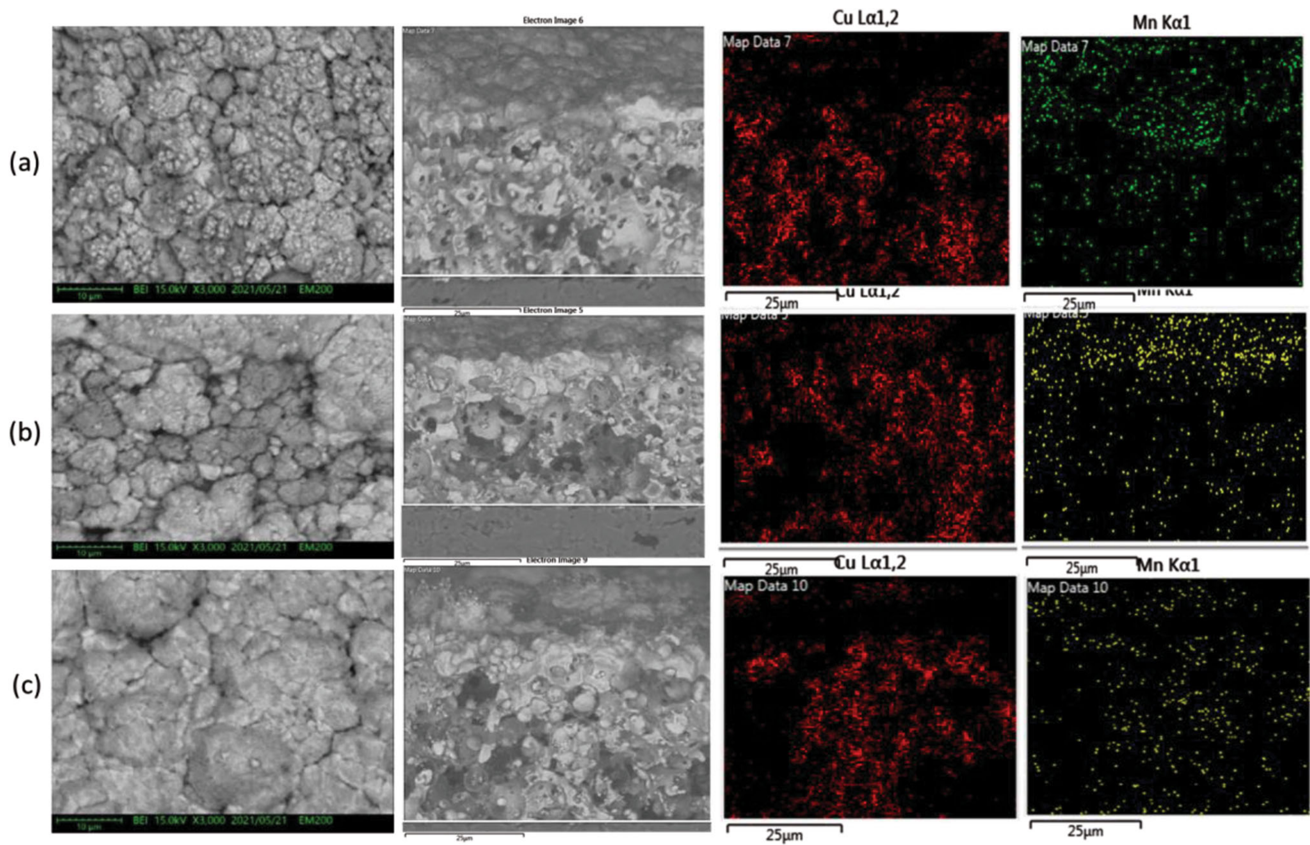

Fig. 11 Microstructure and element mapping of CuMn film (a) before and after annealing at 900 °C for 1 h in (b) N_2 and (c) in N_2-H_2

potential and the activity coefficient of Mn are shown in the following Eq 2.

$$\mu_{Mn} = \mu_{Cu}^{\alpha} + RT\mathrm{Ln}N_{Mn} + RT\ln\gamma_{Mn} \quad \text{(Eq 2)}$$

where μ_{Cu} is the chemical potential of pure Cu, μ_{Mn} is the atomic concentration of Mn, and RT has its usual meaning. According to the equation, the chemical potential and the activity coefficient of Mn are very sensitive to the atomic concentration of Mn.

From the SEM analysis, we could observe that the CuMn films annealed with and without hydrogen in nitrogen performed different morphologies and the oxidation act had an important role during the process. Also, SEM results are corresponding to the results of Raman and XPS, which could provide information for the synthesis of the CuMn alloy. In the following section, the electrical properties would be discussed with the resistivity and TCR.

4. Resistivity and TCR of the CuMn Alloy Film after Annealing

To investigate the electrical properties of the annealed samples with different annealing temperatures, the resistivity of the samples annealed in N_2-H_2 were measured in the range of 25-125 °C as shown in Fig. 12. It is obvious that the resistivity of the CuMn films is abruptly increased to 500 $\mu\Omega$-cm after 700 °C annealing in N_2-H_2. It is attributed to the formation of the CuMn alloy film. It reached the highest resistivity of 1000 $\mu\Omega$-cm when the annealing temperature was 900 °C. The TCR of the films annealed in N_2-H_2 decreased as the annealing temperature increased and it has the lowest TCR of 150 ppm at 900 °C. In fact, the electrical behavior of the CuMn films is closely related to its crystal structure. F. Misják and his coworkers found that the TCR of the CuMn alloy film could decrease due to the resence of the amorphous CuMn (Ref 29). The disordered structures with weakly localized electrons and a very high frequency of scattering would lead to lower conductivity and thermal stability. However, the oxidation would induce the deterioration of the CuMn alloy, resulting in the TCR of a metallic type. It has been reported that the oxidation situation of the CuMn film would occur even it was exposed to the N_2 atmosphere. The low content of oxygen in the nitrogen is enough for the phase transformation from Mn to Mn-oxides. The presence of Mn-oxides would induce the separation between Cu and Mn. Therefore, the resistivity is fixed because the current prefers to flow to the Cu region with low resistance. The remarkable fact for this alloy is that the value of the resistance, its temperature coefficient was largely affected by a small oxidization, since manganese has a large affinity with oxygen. When the alloy is oxidized, the specified temperature, where the temperature coefficient of the resistance of CuMn alloy changes from positive to negative, decreases. The temperature variation of the resistance of the CuMn alloy sensitively depends on the effect of the third element, the oxidization of the surface and the working-up of the specimen (Ref 30).

There are alloys which have the negative temperature coefficient of the resistance, but it should be noted that these

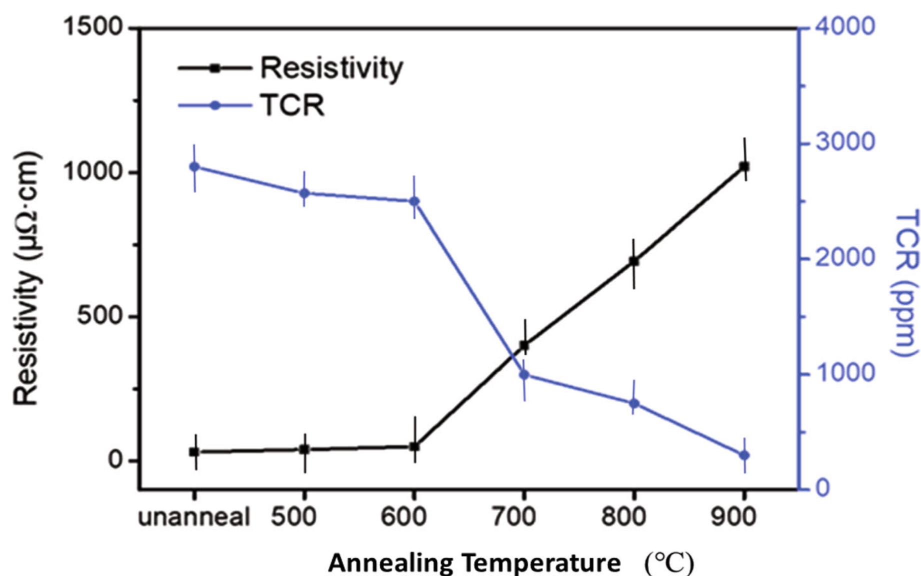

Fig. 12 Resistivity and TCR of CuMn films with different annealing temperatures in N_2-H_2

alloys have one or two transition metals as their constituents. It is well known that the transition metals have the incomplete d-shell and their physical properties, are more complex than other metals. The resistance of the transition metals is determined mainly by the behaviors of the s -electrons, but there is an empty part of d-band, which has considerably larger state density than s-band. The resistance of the transition metals is affected by the transition of the conduction electrons than the s-transition. Hence, when the state density of the Fermi surface of the d-band remarkably decreases with rising temperature in suitable combination of copper and manganese, CuMn alloy has a negative temperature coefficient (Ref 31).

5. Conclusion

In this work, the CuMn alloy film was successfully prepared by electrochemical deposition and post-annealing based on the Cu-Mn structure and the hydrogen-containing annealing atmosphere. The electrodeposited CuMn film annealing at 900 °C in N_2-H_2 shows promising properties including of TCR (150 ppm) with resistivity (1000 $\mu\Omega$-cm).

Well-crystallized Cu thick films were successfully formed via galvanic displacement based on the Al thick films and exhibited preferred (111) orientation with a high density and low resistance. In the CV negative scan, no peaks could be observed and only a violent drop appeared over $-$ 1.5 V, implying that a Mn electroplating reaction was happening. The results revealed that the higher pH value could improve the potential and proper $(NH_4)_2SO_4$ could both prevent the Mn oxidation and increase the nucleation rate of Mn.

Compared to the pure nitrogen annealing atmosphere, the hydrogen-containing environment could not only reduce the oxidation during the post-annealing process but also promote the interdiffusion between the Cu and Mn. The films annealed in N_2-H_2 demonstrated an even and homogeneous surface, implying a good phase transformation of the CuMn alloy film through the Cu-Mn interdiffusion.

Acknowledgments

The author would like to thank Ministry of Science and Technology, Taiwan, for the financial support and gratefully acknowledge Yageo Corp. for supporting equipment to this work.

Author Contributions

W.-H.L. is responsible for concept of investigation, N.G.P. is responsible for analysis and manuscript writing and C.W. Chang is responsible for experiments and measurement.

Data Availability

The data that support the findings of this study are available from the corresponding author upon reasonable request.

Conflict of interest

The authors declare that the research was conducted in the absence of any commercial or financial relationships that could be construed as a potential conflict of interest.

References

1. F. Misják, K.H. Nagy, P. Lobotka and G. Radnóczi, Electron Scattering Mechanisms in Cu-Mn Films for Interconnect Applications, *J. Appl. Phys.*, 2014, **116**(8), p 083507
2. E.M. Kim, S.C. Kim and S. Lee, Electrical Properties of Cu/Mn Alloy Resistor with Low Resistance and Thermal Stability, *J. Korean Inst. Electr. Electron. Mater. Eng.*, 2016, **29**(6), p 365–369
3. A. Bahrami, A. Delgado, C. Onofre, S. Muhl and S.E. Rodil, Structure, Mechanical Properties and Corrosion Resistance of Amorphous Ti-Cr-O Coatings, *Surf. Coat. Technol.*, 2019, **374**, p 690–699
4. J. Lin, H. Jia, H. Liang, S. Chen, Y. Cai, J. Qi, C. Qu, J. Cao, W. Fei and J. Feng, In Situ Synthesis of Vertical Standing Nanosized NiO Encapsulated in Graphene as Electrodes for HighPerformance Supercapacitors, *Adv. Eng. Mater.*, 2018, **20**(3), p 1700687

5. J. Li, A. Du, Y. Fan, X. Zhao, R. Ma and J. Wu, Effect of Shot-Blasting Pretreatment on Microstructures of Hot-Dip Galvanized Coating, *Surf. Coat. Technol.*, 2019, **364**, p 22–31
6. H.M. Hdz-García, R. Muñoz-Arroyo, M. Alvarez-Vera, A. Bahrami, A.I. Mtz-Enriquez, J.C. Díaz-Guillen, F.A. Hernández-García, J.L. Acevedo-Dávila and L. Santiago-Bautista, Wear Resistance of Graphenic-Nickel Composite Coating on Austenitic Stainless Steel, *Mater. Lett.*, 2020, **281**, p 128769
7. H.Y. Lee, C.W. He and Y.C. Lee, The Effect of Yttrium Addition on the Microstructures and Electrical Properties of CuMn Alloy Thin Films, *Coatings*, 2019, **9**(2), p 118
8. R. Baghi, G.R. Peterson and L.J. Hope-Weeks, Thermal Tuning of Advanced Cu Sol–Gels for Mixed Oxidation State Cu/Cu x O y Materials, *J. Mater. Chem. A*, 2013, **1**(36), p 10898–10902
9. H.Y. Cheng, D.P. Tran, K.N. Tu and C. Chen, Effect of Deposition Temperature on Mechanical Properties of Nanotwinned Cu Fabricated by Rotary Electroplating, *Mater. Sci. Eng. A*, 2021, **811**, p 141065
10. M. Haerifar and M. Zandrahimi, Effect of current density and electrolyte pH on microstructure of Mn-Cu electroplated coatings, *Appl. Surf. Sci.*, 2013, **284**, p 126–132
11. T.C. Kuo, C.R. Kuo and W.H. Lee, A Novel Method to Fabricate a Thick-Film Cu Electrode Fired in Air Through Printing Al Electrode and Reduction-Oxidation Substitution Reaction, *IEEE Trans. Compon. Packag. Manuf. Technol.*, 2021, **11**(3), p 485–492
12. W.H. Lee and K.C. Chung, Investigation of a Copper–Nickel Alloy Resistor Using Co-Electrodeposition, *J. Appl. Electrochem.*, 2020, **50**, p 535–547
13. M. Ishikawa, H. Enomoto, N. Mikamoto, T. Nakamura, M. Matsuoka and C. Iwakura, Preparation of Thin Film Resistors with Low Resistivity and Low TCR by Heat Treatment of Multilayered Cu/Ni Deposits, *Surf. Coat. Technol.*, 1998, **110**(3), p 121–127
14. J. Liu, C. Yang, P. Zou, R. Yang, C. Xu, B. Xie, Z. Lin, F. Kang and C.P. Wong, Flexible Copper Wires Through Galvanic Replacement of Zinc Paste: A Highly Cost-Effective Technology for Wiring Flexible Printed Circuits, *J. Mater. Chem. C*, 2015, **3**(32), p 8329–8335
15. J. Winiarski, A. Leśniewicz, P. Pohl and B. Szczygieł, The Effect of pH of Plating Bath on Electrodeposition and Properties of Protective Ternary Zn-Fe-Mo Alloy Coating, *Surf. Coat. Technol.*, 2016, **299**, p 81–89
16. J. Gong and G. Zangari, Electrodeposition and Characterization of Manganese Coatings, *J. Electrochem. Soc.*, 2022, **149**(4), p 209–217
17. D.A. Brevnov, T.S. Olson, G.P. López and P. Atanassov, Electroless Deposition of Silver by Galvanic Displacement on Aluminum Alloyed with Copper, *J. Phys. Chem. B*, 2004, **108**, p 17531–17536
18. W.S. Chiang, J.Q. Huang, P.C. Chen, P.W. Wu, A. Joi and Y. Dordi, Pulse Electrodeposition of Copper-Manganese Alloy in Deep Eutectic Solvent, *J. Alloy. Compd.*, 2018, **742**, p 38–44
19. J.S. Fang, S.L. Sun, Y.L. Cheng, G.S. Chen and T.S. Chin, Cu and Cu(Mn) Films Deposited Layer-by-Layer Via Surface-Limited Redox Replacement and Underpotential Deposition, *Appl. Surf. Sci.*, 2016, **364**, p 358–364
20. S.H.R. Davies and J.J. Morgan, Manganese(II) oxidation Kinetics on Metal Oxide Surfaces, *J. Colloid Interface Sci.*, 1989, **129**(1), p 63–77
21. C.Y. Wu, C.T. Wu, W.H. Lee, S.C. Chang and Y.L. Wang, A Study on Annealing Mechanisms with Different Manganese Contents in CuMn Alloy, *J. Alloys Compd.*, 2012, **542**(25), p 118–123
22. H. Okamoto, Supplemental Literature Review of Binary Phase Diagrams: Ag-Ni, Ag-Zr, Au-Bi, B-Ni, Co-Sb, Cu-Mn, Cu-Si, Cu-Zn, Fe-Zr, Li-Sb, Mg-Pu, and Si-Zr, *J. Phase Equilib. Diffus.*, 2018, **39**, p p87-100
23. R. Mariappan, V. Ponnuswamy and P. Suresh, Effect of Doping Concentration on the Structural and Optical Properties of Pure And Tin Doped Zinc Oxide Thin Films by Nebulizer Spray Pyrolysis (NSP) Technique, *Superlattices Microstruct.*, 2012, **52**(3), p 500–513
24. S. Dey and G.C. Dhal, Synthesis of Hopcalite Catalysts by Various Methods for Improved Catalytic Conversion of Carbon Monoxide, *Mater. Sci. Energy Technol.*, 2020, **3**, p 377–389
25. Y. Wang, L. Cao, N.J. Libretto, X. Li, C. Li, Y. Wan, C. He, J. Lee, J. Gregg, H. Zong, D. Su, J.T. Miller, T. Mueller and C. Wang, Ensemble Effect in Bimetallic Electrocatalysts for CO_2 Reduction, *J. Am. Chem. Soc.*, 2019, **141**, p 16635–16642
26. A.F. da Silva Jr, A.S. Martins and M.F. de Campos, Longe Range Exchange Interactions in Sintered CuMn Alloys: A Monte Carlo Study, *Mater. Sci. Forum*, 2017, **899**, p 266–271
27. Y. Cui, A. Dong, Qu. Yanbin, J. Zhang, M. Zhao, Z. Wang and Q. Jiang, Theory-Guided Design of Nanoporous CuMn Alloy for Efficient Electrocatalytic Nitrogen Reduction to Ammonia, *Chem. Eng. J.*, 2021, **426**, p 131843
28. J. Iijima, Y. Fujii, K. Neishi and J. Koike, Resistivity Reduction by External Oxidation of Cu-Mn Alloy Films for Semiconductor Interconnect Application, *J. Vac. Sci. Technol. B Microelectron. Nanometer Struct. Process. Meas. Phenom.*, 2009, **27**(4), p 1963–1968
29. G. Wang, Z. Ye, L. Zhao, Y. Liu, J. Ji and J. Wang, Catalytic Ozonation of Toluene Over Amorphous Cu-Mn Bimetallic Oxide: Influencing Factors, Degradation Mechanism and Pathways, *Chemosphere*, 2022, **307**(4), p 135993
30. S.Y. Joo, Y. Choi and H.C. Shin, Hierarchical Multi-porous Copper Structure Prepared By Dealloying Electrolytic Copper-Manganese Alloy, *J. Alloys Compd.*, 2022, **900**, p 163423
31. P.K. Khowash and D.C. Khan, Electronic Structure Calculation of CuMn Alloy, *J. Phys.*, 1991, **36**(2), p 185–218

Publisher's Note Springer Nature remains neutral with regard to jurisdictional claims in published maps and institutional affiliations.

Springer Nature or its licensor (e.g. a society or other partner) holds exclusive rights to this article under a publishing agreement with the author(s) or other rightsholder(s); author self-archiving of the accepted manuscript version of this article is solely governed by the terms of such publishing agreement and applicable law.